Original scientific papers UDK 621.384.8:539.1.078
DOI 10.7251/COMEN2102140K

TOWARD LOW-ENERGY SPARK PLASMA SINTERING OF HOT-DEFORMED Nd-Fe-B MAGNETS

Matic Korent [1,2,], Marko Soderžnik [1,3], Urška Ročnik[1], Sandra Drev[4], Kristina Žužek Rožman[1,2], Sašo Šturm[1,2], Spomenka Kobe[1,2*], Kristina Žagar Soderžnik[1]*

[1] Jožef Stefan Institute, Department for nanostructured materials, Jamova cesta 39, Ljubljana, Slovenia
[2] Jožef Stefan International Postgraduate School, Jamova cesta 39, Ljubljana, Slovenia
[3] Laboratory for Tribology and Interface Nanotechnology (TINT), Faculty for Mechanical Engineering, University of Ljubljana, Ljubljana, Slovenia
[4] Center for Electron Microscopy and Microanalysis, Jožef Stefan Institute, Jamova cesta 39, Ljubljana, Slovenia

Abstract: In this work, we present a newly developed, economically efficient method for processing rare-earth Nd-Fe-B magnets based on spark plasma sintering. It makes us possible to retain the technologically essential properties of the produced magnet by consuming about 30% of the energy as compared to the conventional SPS process. A magnet with anisotropic microstructure was fabricated from MQU F commercial ribbons by low energy consumption (0.37 MJ) during the deformation process and compared to the conventionally prepared hot-deformed magnet, which consumed 3-times more energy (1.2 MJ). Both magnets were post-annealed at 650 °C for 120 min in a vacuum. After the post-annealing process, the low-energy processing (LEP) hot-deformed magnet showed a coercivity of 1327 kAm^{-1}, and remanent magnetization of 1.27 T. In comparison, the high-energy processing (HEP) hot-deformed magnet had a coercivity of 1337 kAm^{-1} and a remanent magnetization of 1.31 T. Complete microstructural characterization and detailed statistical analyses revealed a better texture orientation for the HEP hot-deformed magnet processed by high energy consumption, which is the main reason for the difference in remanent magnetization between the two hot-deformed magnets. The results show that, although the LEP hot-deformed magnet was processed by three times lower energy consumption than in a typical hot-deformation process, the maximum energy product is only 8 % lower than the maximum energy product of a HEP hot-deformed magnet.

Keywords: hot-deformed Nd-Fe-B magnets, low energy processing hot-deformation process, spark plasma sintering, statistical analyses, electron microscopy

1. INTRODUCTION

Discovered in 1984 [1,2], Nd-Fe-B magnets are permanent magnets that have the highest maximum energy product $(BH)_{max}$, more than 400 kJm^{-3}, which is close to the theoretical limit of 512 kJm^{-3}[3–7]. Thus, they are in very high demand for major applications in electric (hybrid) vehicles, traction motors, and wind turbines [8,9]. The $Nd_2Fe_{14}B$ has a tetragonal crystallographic structure with a $P4_{2/mnm}$ space group [10]. To achieve a large remanent magnetization ($\mu 0Mr$) and consequently a large value of $(BH)_{max}$ of a magnet with such a composition, a high degree of (001) texture must be achieved [11,12]. In addition, a high-volume percentage of the $Nd_2Fe_{14}B$ phase, low oxygen content, low amount of non-ferromagnetic material and small crystallite size, near single domain size (~ 250 nm), is desired [13]. Besides the sintering of magnetically pre-aligned particles, the hot-deformation (HD) process is a method in which the grain boundary migration and sliding of planes are induced by plastic deformation [11,12,14]. In 1985, Lee et al. and Tang et al. [15–17] produced HD magnets with an ultrafine microstructure of average grain size, from 300 nm to 400 nm, from melt-spun

* Corresponding author: matic.korent@ijs.si

Nd-Fe-B ribbons. The rapidly solidified powder with randomly orientated nanocrystals was transformed into textured, closely packed, plate-like grains with a high degree of c-axis crystallographic alignment along the pressing direction during the HD process, resulting in a large $\mu 0Mr$ [18,19]. Recently, Tang et al. prepared the ribbons with low addition of Nb (0.29 wt.%) and performed the HD process at 850 °C to obtain a HD magnet with 75 % height reduction and $\mu 0Mr$ of 1.45 T, which is comparable to the values of sintered magnets [11].

The coercivity ($\mu 0Hc$) of HD magnets, strongly depends on the homogenous distribution of Nd-rich phases around $Nd_2Fe_{14}B$ grains [21]. Sufficient magnetic isolation effectively enhances the value of coercivity with the reduction of exchange coupling between the $Nd_2Fe_{14}B$ grains [21,22]. Furthermore, it acts as a barrier to prevent a domain wall–motion during the magnetization reversal process [12,23,24]. However, detailed microstructure investigations by Lewis et al. and Liu et al. showed that the Nd-rich intergranular phase contains up to 50 at.% ferromagnetic elements (pure metals of Fe and Co), which suggests the ferromagnetic nature of the isolation phase and consequently the exchange coupling between $Nd_2Fe_{14}B$ grains [21,25,26]. As a consequence, Liu et al. showed that heavy rare earth (HRE)-free HD magnets could achieve $\mu 0Hc$ only up to 1430 kAm^{-1} at room temperature (RT) [21].

In addition to microstructure characteristics, processing conditions have a significant impact on the magnetic properties of HD magnets. According to Hioki et al., both the reduction ratio and hot-deformation temperature define the final $\mu 0Mr$, $\mu 0Hc$, and $(BH)_{max}$ [27]. The value of $\mu 0Mr$ is closely related to the reduction ratio as established by Korent et al. [28]. The increase in $\mu 0Mr$ is proportional to the reduction ratio due to the higher degree of texture and a predominant c-plane growth in $Nd_2Fe_{14}B$ grains [12,27]. Additionally, the working temperature is also important in terms of grain growth as it causes a deterioration of the magnetic properties [27].

Typically, HD magnets are made by carrying out the hot-press (HP) method (Figure 1a) where the heating rates are rather low: 5–10 °C min^{-1} [29]. The HP technique is a combination of resistance or induction heating and the pressure applied on a sample. Usually, the system includes a coil and the heating is based on induction or electrical resistance heating [30]. Another option for similar processing is the spark plasma sintering (SPS) (Figure 1b), in which the densification process is simultaneously applied by a uniaxial pressure and a high direct current (DC) pulse [29]. The application of a mechanical force is similar to that in the HP process. Meanwhile, the heating rates, up to 1000 °C min^{-1}, are much higher in comparison to the HP [29]. Efficient and fast densification in the SPS method occurs through a combination of Joule heating, the action of spark discharge, the plastic deformation effect, and the diffusion of material [31]. According to Chawake et al., Joule heating is a primary source of heat during the densification of metal powders [32]. The heating occurs due to the electric resistance, which is the most significant at the contact between the particles [32]. Consequently, the SPS process enables ultra-fast sintering at low temperatures and short holding times to full material density, which preserves the magnetic properties and reduces the power consumption of the process itself [33,34].

In this work, the SPS method was used to fabricate a fully dense HD Nd-Fe-B magnet with a high deformation ratio below-energy processing (LEP) SPS method. We studied the microstructure and its influence on the final magnetic properties and compared the results to a microstructure of an HD magnet produced by the high-energy processing (HEP) SPS method.

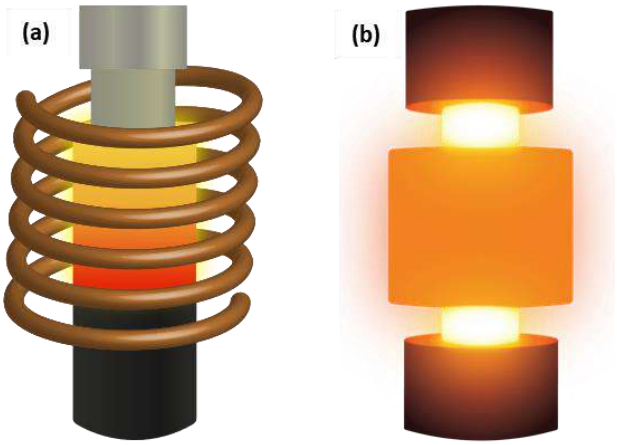

Figure 1. Schematic presentation of (a) HP method and (b) SPS method

2. EXPERIMENTAL

Commercial (MQU-F) Nd-Fe-B melt-spun ribbons with the nominal composition of $Nd_{30.1}Pr_{0.4}Fe_{62.0}Co_{6.1}Ga_{0.5}B_{0.9}$ (wt.%) were used for the HD process. MQU-F ribbons were first hot-pressed (HP) into a fully dense magnet using a spark plasma sintering (SPS) furnace (Fuji Electronic Industrial Dr Sinter SPS Syntex 3000). The magnet was compacted in a 10 mm graphite mould at SPS temperature 675 °C under a uniaxially applied pressure of 50 MPa in a vacuum ($\approx 5\times10^{-2}$ mbar). The SPS temperature was controlled by a K-type thermocouple inserted into the graphite mould at the level of the sample. The

thickness of the graphite wall splitting the thermocouple from the sample was minimal (≈1 mm). A 12:2 on-off direct current (DC) pulse sequence was applied to heat the sample. After the sintering process was finished, the pressure was immediately released and the mould with the sample was cooled to RT by cooling water circulating through the system. The density of the HP magnet was determined by a bulk density measurement system (Densitec, Exelia AG, Switzerland).

The HP magnets were subsequently HD in a 20 mm graphite mould at two different maximum SPS temperatures in a vacuum. The describing temperatures below are the nominal temperatures and serve as an SPS processing parameter to determine energy consumption through the deformation process. The SPS settings and measurement were equal to the HP process described in the previous paragraph. For processing the LEP HD magnet, the SPS temperature was set at nominal 350 °C, and for the HEP HD magnet, at nominal temperature of 680 °C. In the first case (LEP HD magnet), the heating rate from RT to nominal temperature 300 °C was 100 °Cmin^{-1}, followed by a lower heating rate of 30 °Cmin^{-1} and 20 °Cmin-1in the next 2 minutes to minimize the overshooting. At the last minute, the temperature was maintained at the target value. The higher pressure was initially applied at a nominal temperature of 250 °C, and within 3.5 min, it constantly increased to a maximum pressure of 90 MPa. After the target temperature was reached, the sintering process was immediately stopped and pressure released. Meanwhile, in the second case (HEP HD magnet), the heating rate from RT to 600 °C was 75 °Cmin^{-1}, followed by a lower heating rate of 60 °Cmin^{-1} and 20 °Cmin^{-1} in the next 2 minutes to prevent the overshooting. At the last minute, the temperature was maintained at the target value, and the maximum pressure of 90 MPa was applied during this holding time. As prepared, HD magnets were subjected to the post-annealing process at 650 °C for 120 min in a vacuum. The magnetic properties of both HP (SPS)-ed HD magnets before and after annealing were measured with a permeameter (Steingroever EP2) at RT. The respective deformation ratios of the LEP HD and HEP HD magnets were 71 % and 75 %. The deformation ratio (%) is defined as:

$$DR = \left(\left(h_{HP} - h_{HD} / h_{HP}\right) \cdot 100\%\right) \quad (1)$$

where DR is the deformation ratio (%) and h_{HP}, h_{HD} are the heights of the HP, HD magnet (mm).

The X-ray powder diffraction data were collected from the sample surface perpendicular to the pressing direction with a Malvern Panalytical Empyrean X-ray diffractometer (XRD) using monochromated X-Rays, produced by a Cu-target tube (0.15406 nm). The scan range in Bragg angles was from 10 ° to 90 ° (2θ). The XRD data were analysed by HighScore Plus XRD Analysis Software. The microstructural characterization using scanning electron microscopy (SEM) was performed to study the influence of SPS temperature and pressure on the HD process. The samples were cut into smaller square blocks and the surface parallel to the pressing direction was metallographically polished. After polishing, the surface was chemically etched with 3 M Cyphos solution for 10 s and then intensively washed with ethanol. For SEM microstructural characterization, samples were analyzed using a high-resolution, field-emission gun SEM (FEG-SEM) Thermo Fisher, Verios G4 HP. The acquired images were statistically processed by the ImageTool program to determine the difference in the grain size and aspect ratio, as measured between the long and short axis of the anisotropic Nd2Fe14B grains of HD magnets. Detailed microstructural investigations of the samples were performed by transmission electron microscopy (TEM) using a 200 kV microscope (TEM; JEM-2100, Jeol, Japan). For TEM bulk sample investigations, the sample was cut into square blocks of 1.8 x 1.8 mm, perpendicular and parallel to the pressing direction, respectively. The blocks were fitted into 3 mm brass cylinders using epoxy glue to improve strength. The TEM specimen was ground to a thickness of 100 μm and dimpled down to 15 μm at the disc centre (Dimple grinder, Gatan Inc., Warrendale PA, USA). TEM specimen was finally ion-milled (PIPS, Precision Ion Polishing System, Gatan Inc., USA) using 3 kV Ar+ ions at an incidence angle of 8° until perforation.

3. RESULTS

3.1. LEP vs HEP HD magnet

Two differently prepared HD magnets are distinguished based on the energy consumption for the deformation process. Figure 2 shows electric power (P) consumption during the SPS process of the LEP and HEP HD magnets. The used energy consumption is the time integral of the electric power, and its value was obtained from the area below the curves. During the deformation process of the LEP HD magnet, the consumed energy was 0.37 MJ, which is more than 3-times less compared to 1.2 MJ consumed energy in the HEP HD process.

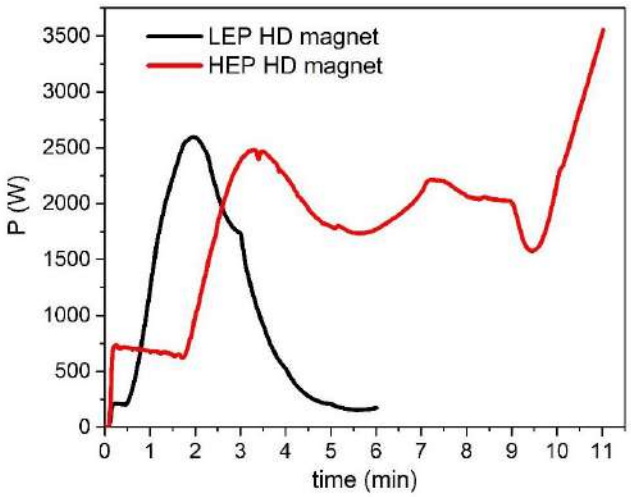

Figure 2. Electric power (P) consumption during the SPS process of LEP HD (black curve) and HEP HD magnet (red curve). The area under the curve was obtained from numerical integration $\int_0^{t_{end}} P \cdot dt$. The calculated energy consumptions are 0.37MJ for LEP and 1.2 MJ for HEP HD, respectively

3.2. Magnetic properties

Figure 3 shows the demagnetization curves of LEP and HEP HD magnets before and after post-annealing treatment at 650 °C for 120 min. Note that magnets were fully magnetized in a pulse magnetizer with 6 T before each measurement.

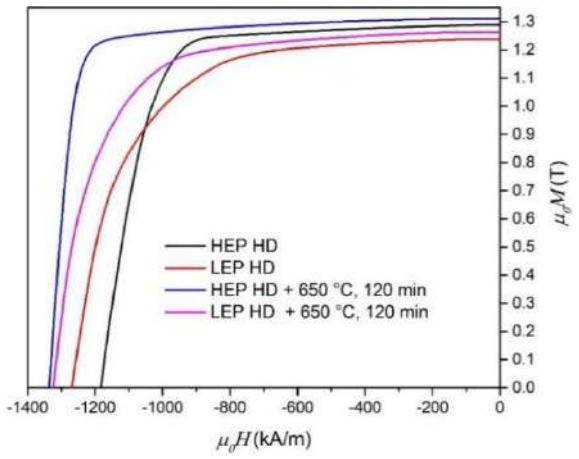

Figure 3. Demagnetization curves of LEP HD magnet (red curve) and HEP HD magnet (black curve) and demagnetization curves of LEP (purple curve) and HEP (blue curve) HD magnets after the post-annealing process at 650 °C for 120 min

The magnetic properties and the squareness (Q) of the demagnetizing curves of each HD magnet are collected in Table 1. The $\mu_0 M_r$ of the LEP HD magnet was enhanced with post-annealing treatment from 1.24 T to 1.27 T, and $\mu_0 H_c$ from 1271 kAm^{-1} to 1327 kAm^{-1}. A similar improvement after post-annealing in $\mu_0 M_r$, from 1.29 T to 1.31 T, was also observed in the HEP HD magnet. Meanwhile, the enhancement in coercivity of HEP HD magnet after the post-annealing process was more significant – from 1184 kAm^{-1} to 1337 kAm^{-1}. The squareness of the demagnetizing curves was also improved after additional heating. In the case of LEP HD magnet, the squareness was enhanced from 70 % to 77 %, and from 82 % to 91 % in the case of the HEP HD magnet. The squareness is defined as:

$$Q = \mu_0 H_k / \mu_0 H_c \cdot 100\% \quad (2)$$

where μ0Hkis a field value corresponding to the location of the knee point in the intrinsic curve at 90 % of $\mu_0 M_r$ [35].

Table 1. Magnetic properties (μ0Hc, μ0Mr, (BH)max) and Q of the demagnetizing curves of LEP, HEP HD magnets and of LEP, HEP HD magnets after the post-annealing process at 650 °C for 120 min.

	LEP HD magnet	HEP HD magnet	LEP HD magnet + 650 °C, 120 min	HEP HD magnet + 650 °C, 120 min
μ0Hc (kAm^{-1})	1271	1184	1325	1337
μ0Mr (T)	1.24	1.29	1.27	1.31
$(BH)_{max}$ (kJm^{-3})	295	320	310	335
Q (%)	70	82	77	91

3.3. Microstructural characterization

Figure 4 shows the XRD patterns of LEP and HEP HD magnets after the post-annealing process. The analysis was performed on the surface perpendicular to the pressing direction. The characteristic peaks with direction (004), (105), (006), and (008) of anisotropic microstructure are labelled in the chart.

Backscattered electron (BSE)-SEM characterization was performed on the central part of LEP and HEP HD magnets to understand the influence of microstructure on the magnetic properties. Figure 5 shows cross-section images of (a) LEP and (b) HEP HD magnets after the post-annealing process, where the direction of the c-axis is the same as the pressure direction. It is to note that BSE-SEM results of LEP and HEP HD magnets before annealing process gave identical results. In both images, coarse grains and grains with random orientation can be seen, especially in the LEP HD magnet. The main difference between those two magnets is in the microstructure texturing. A HEP HD magnet has a stronger c-axis alignment of the Nd2Fe14B grains along the pressing direction than the LEP HD magnet, which will be confirmed later

with more detailed information about the grains' shape and orientation.

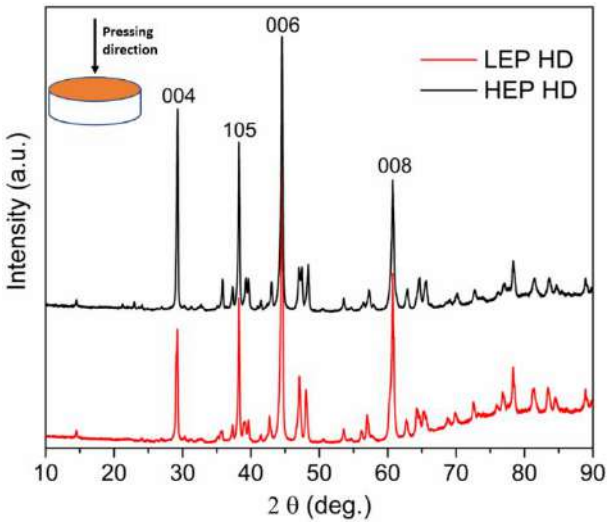

Figure 4. XRD patterns of LEP and HEP HD magnets after the post-annealing process

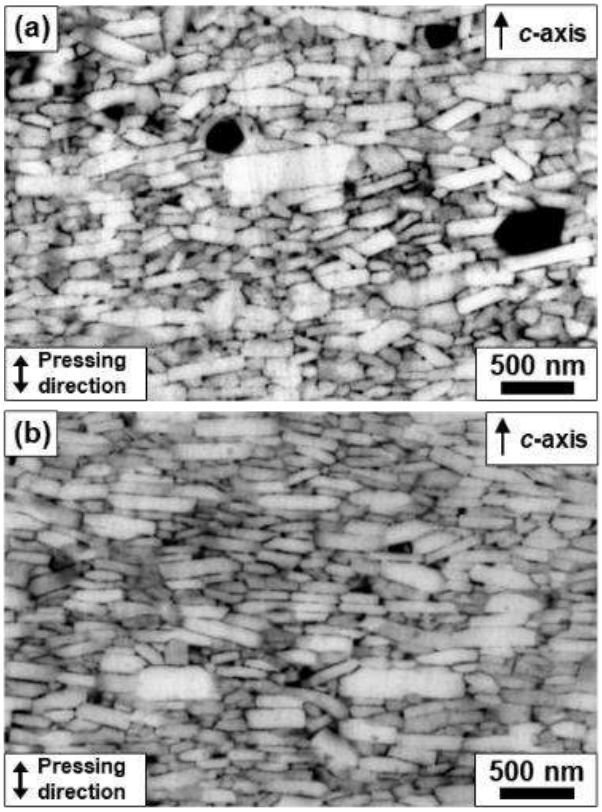

Figure 5. BSE-SEM images of (a) LEP and (b) HEP HD magnet (The SEM characterization were performed after the post-annealing process)

Based on BSE-SEM images, histograms, and standard distribution curves were obtained by counting the width and height of 200 characteristic grains, which are not overlapped by others. Figure 6 shows the height and width distribution of respective post-annealed LEP HD magnet (a, b) and HEP HD magnet (c, d). The LEP HD magnet has a broader grain height distribution with an average height of 63 nm (Figure 6a), compared to the HEP HD magnet with an average height of 67 nm (Figure 6c). In the LEP HD magnet, 5 % of grains are larger than 160 nm, which is not the case in the HEP HD magnet. In contrast, the width distribution curve of the HEP HD magnet (Figure 6d) is broader, with a more significant number of long grains and an average width of 348 nm. Almost 100 nm lower, the average grain width of 252 nm is observed in the LEP HD magnet (Figure 6b).

The aspect ratio (width/height) was calculated based on each grain's width and height. Figure 7 a, c presents the histograms and distribution of aspect ratios of 200 grains, where (a) illustrates the LEP and (c) the HEP HD magnets after post-annealing. The standard distribution curve of the analyzed grains from the HEP HD sample is broader, with an average aspect ratio of ~5.3. The LEP HD sample possesses mainly grains with an aspect ratio between 2 and 6.5 and subsequently has a narrower distribution curve. The average aspect ratio is consequently lower, at ~4.2. Figure 7 also shows the angle between the pressing direction and the c-axes of particular grains of (b) the LEP and (d) the HEP HD samples after post-annealing. In this case, the grain distribution curve in the sample LEP HD is broad, which means that many grains are oriented out of the pressing direction. The average deviation angle is 8.3°. The HEP HD sample has a narrower distribution curve and a smaller number of grains with a high deviation angle from the pressing direction. The average deviation angle is 7.4°, which is almost 1° lower than in the LEP HD sample.

Detailed TEM analysis (Figure 8) with selected area electron diffraction patterns (SAED) was performed parallel and perpendicular to the pressing direction of LEP and HEP HD samples after the post-annealing process. Figure 8 (a, b) shows grains parallel to the c-axis. The low magnification images show the size and shape of anisotropic grains that correspond to the SEM findings. Analysis of the grains determined misalignment of ± 2-3 degrees in relation to the preferential plane. By detailed analysis of diffraction patterns, we confirmed that the preferred orientation of the grains is in (0-10) direction for both LEP and HEP HD magnets.

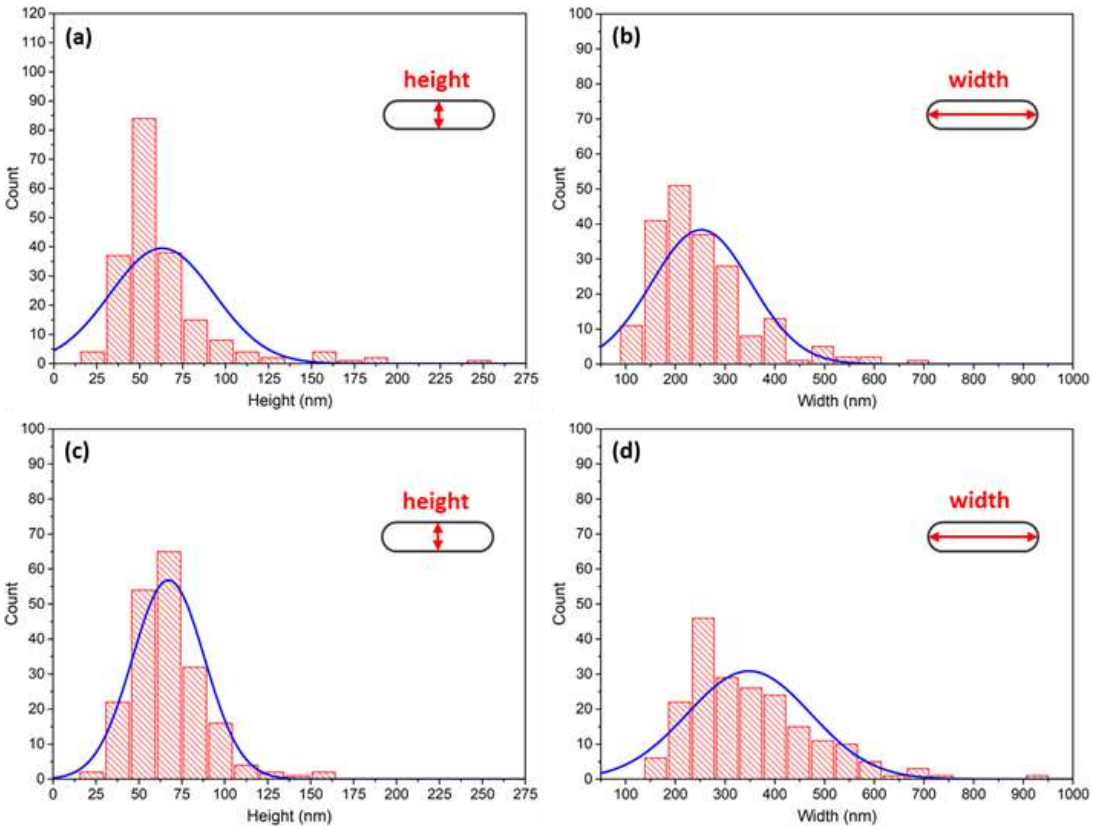

Figure 6. The statistic distribution of the height and width of 200 grains of the (a), (b) LEP and (c), (d) HEP HD magnets (All statistic distributions were performed on the samples after the post-annealing process)

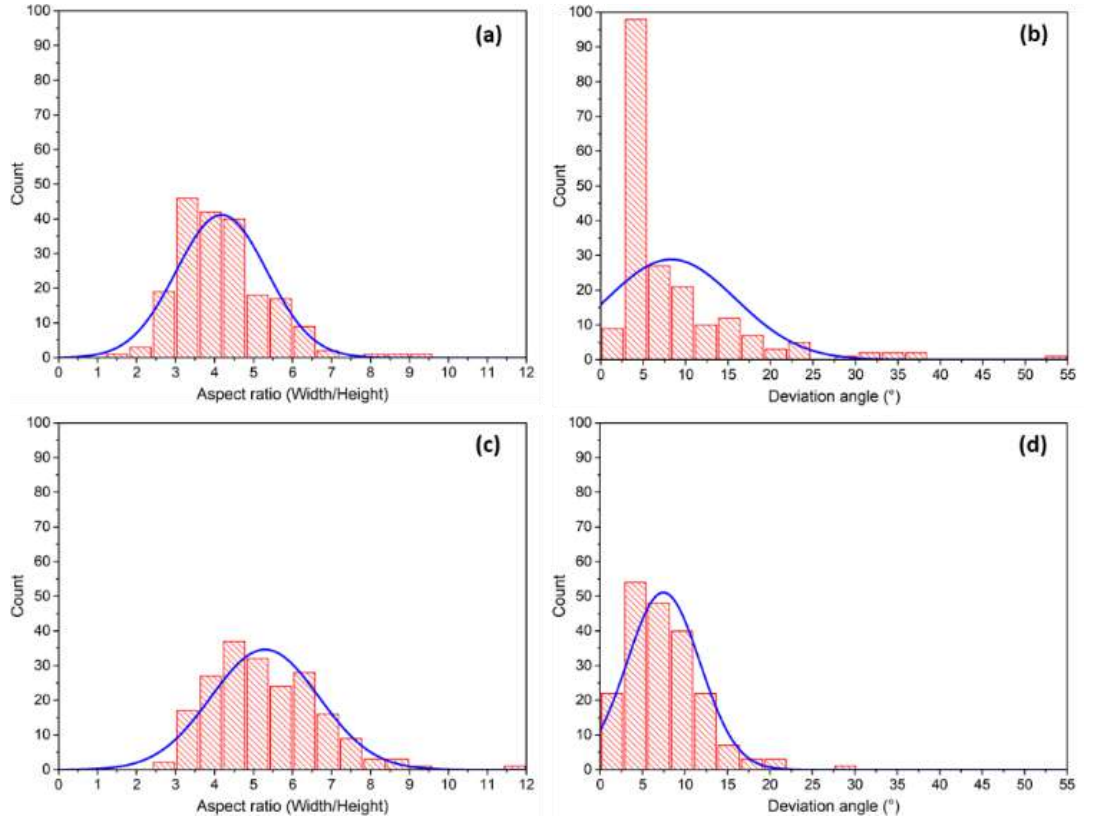

Figure 7. The statistic distribution of the aspect (width/height) ratio and deviation angle of 200 grains of (a), (b) LEP and (c), (d) HEP HD magnet (All statistic distributions were performed after the post-annealing process)

Figure 8 (c, d) shows grains perpendicular to the c-axis. Low magnification images of the LEP and HEP HD samples revealed the idiomorphic shape of grains with a diameter from 0.1 - 0.8 μm. Analysis of the grains determined misalignment of ± 1-2 degrees from a preferential plane. Detailed analysis of diffraction patterns shows the preferential [001] plane of the grains that are related to XRD analysis.

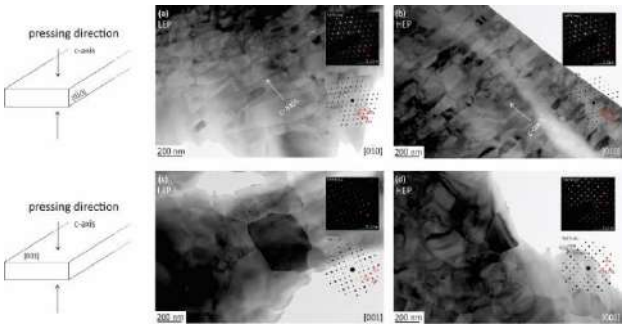

Figure 8. TEM analysis and SAED diffraction patterns (experimental and simulated) of (a) and (c) LEP HD and (b) and (d) HEP HD samples. The analysis was performed parallel and perpendicular to the c-axis (pressing direction)

4. DISCUSSION

This work shows that the amount of energy transferred to the sample influences the temperature gradient in the hot-deformation process. Lower energy should be reflected in a lower average temperature of the sample, which is in the experiment compensated by applying a specific pressure regime, making the desired microstructure transformations possible.

The HEP HD magnet was processed at the nominal temperature comparable to previously set temperatures using the same technique and material; for example, S. Liu et al. produced an HD magnet at 700 °C [36] and Z.H. Hu et al. at 650–750°C [37]. We showed that the consumed energy during the deformation process is strongly related to the temperature regime, which indicates that a large amount of energy is consumed in a typical hot-deformation process. If the deformation temperature is lower, a large amount of energy can be saved. In our case, during the deformation of the LEP HD, 0.37 MJ of energy was consumed, while the HEP HD magnet processing consumed three times more energy. We performed the XRD analysis perpendicular to the c-axis on LEP and HEP HD magnets to confirm c-axis crystallographic alignment. The XRD patterns of LEP and HEP HD magnets after the post-annealing process show the enhanced intensity of characteristic peaks (004), (006), (008), and (105), which indicates the development of c-axis crystallographic alignment [38]. Parallel to XRD, the TEM analysis was also performed. The diffraction of patterns of the LEP and HEP HD samples coincide with the XRD results, which is an additional indicator of anisotropic microstructure. From the perspective of magnetic properties, we achieved high deformation of ~71 % in the LEP HD magnet and ~75 % in the HEP HD magnet. Hioki et al. showed that the $\mu_0 M_r$ of an HD magnet changed between 70 % and 75 % of height reduction only by 0.02 T, and it remained unchanged above 75 % [27]. Consequently, we can assume that, in our case, the reduction in height partially influences the $\mu_0 M_r$ on HD magnets. However, despite the considerable reduction in height of the HD magnets, there is still a visible difference of 0.05 T in $\mu_0 M_r$ between the LEP HD magnet (1.24 T) and HEP HD magnet (1.29 T) which can be attributed to the uniformity of grains shape and orientation. The texture formation mechanism for plate-like grain growth and alignment can be described by a solution-precipitation-creep model with the assistance of the Nd-rich phase [39–41]. Leonowicz et al. considered that the liquidation of Nd-rich grain boundary phases induces the sliding of grains under applied shear stress, which results in magnets deformation and texture formation [42]. To understand the origin of the difference in magnetic properties between LEP and HEP HD magnets, the shape and orientation of particular grains in the microstructure were investigated. In the case of the HEP HD magnet, the plate-like shape grains have a relatively uniform shape and orientation of the c-axis parallel to the pressing direction. On the other hand, in the LEP HD magnet, the plate-like shape grains have a less uniform shape and more scattered orientation. Castle et al. [43] reported that the reason for the uniform microstructure of HD magnet is a more even temperature distribution across the powder flakes during the sintering. This implies that in the case of processing the LEP HD magnet, the temperature was uneven throughout the sample, which caused the non-uniformity in the final microstructure.

The above-described findings were supported by the counted data, where the results showed a higher aspect ratio between the width and height of grains in the HEP HD magnet's microstructure. The average aspect ratio of ~5.3 was significantly higher than that for the LEP HD magnet (~4.2). The aspect ratio is closely connected to the deformation degree, which gives a partial explanation of the higher $\mu_0 M_r$ and lowers $\mu_0 H_c$ of the HEP HD magnet [12], [40].

To better understand the 0.05T difference in $\mu_0 M_r$, we also measured the angle between the c-axis of the grains and the pressing direction for 200 grains from each HD magnet. Just as with the aspect ratio, the result showed a better grain orientation in the HEP HD magnet. The average deviation angle from the pressing direction is almost 1° lower than for the LEP HD magnet, 8.3°. This indicates better grain orientation for the HEP HD magnet and, consequently, higher $\mu_0 M_r$ and higher $(BH)_{max}$ [40]. From this set of analyzed data, we can also infer the shape of the demagnetization curve. Diverse grain shapes and their more imperfect orientations have a crucial impact on the reduced squareness of the LEP HD magnet [35].

From the perspective of $\mu_0 H_c$, the MQU-F ribbons were chosen for the deformation process due to their rich Nd content. There is 30.1 wt.% Nd in the material composition, which is 4.1 wt.% above the stoichiometric point. Liu et al. showed that within ribbons with high Nd content, the Nd-rich phase fraction increased along the grain boundaries [21]. Due to the increase of Nd content and decrease of Fe and Co content in the grain boundaries, better isolation of $Nd_2Fe_{14}B$ grains is established, which results in a higher value of $\mu_0 H_c$ [21]. The value of $\mu_0 H_c$ is higher for the LEP HD magnet, 1271 kAm^{-1}, compared to the value for the HEP HD magnet, 1184 kAm^{-1}. After the additional post-annealing step at 650 °C for 120 min, all of the magnetic properties were enhanced, presumably due to the removal of internal stress or/and defects [44]. The $\mu_0 M_r$ and $\mu_0 H_c$ of the LEP HD magnet were increased for 0.3 T and 54 kAm^{-1} compared to those of the HEP HD magnet, 0.2 T and 153 kAm^{-1}. According to Yin et al., the inherited crystalline orientation and improved texture promote the remanent magnetization after the post-annealing process [45].

Meanwhile, the post-annealing process coercivity promotion is mainly related to the Nd-rich phase enhanced distribution at the grain boundaries and the ribbon boundaries [45]. The respective LEP HD and HEP HD magnet squareness was improved from 70 % to 77 %, and 82 % to 91 %. The microstructure homogeneity through the grain size distribution, grain shape, grain surface, and spatial distribution is improved by a post-annealing process, which is also the main reason for enhanced squareness [35,46]. Based on the statistical analyses, BSE-SEM and TEM images, the HEP HD magnet's microstructure is more homogenous than the microstructure of the LEP HD magnet, which indicates a better squareness. Given the magnetic properties figure of merit improvement, both HD magnets exhibited ~5 % higher value of (BH)max after the post-annealing process.

5. CONCLUSIONS

In this work, LEP and HEP HD magnets were processed by using an SPS technique, which is significantly lower energy consumption regarding the typical hot-deformation process. We investigated the microstructural and magnetic properties of LEP and HEP HD magnets and performed a detailed analytical comparison. Before the characterization, the post-annealing step of both HD magnets was performed to further enhance the magnetic properties. A LEP HD magnet inhibits just 0.04 T lower remanent magnetization than a HEP HD magnet (1.31 T). After post-annealing, coercivity of the values of both magnets are similar – 1325 kAm^{-1} for the LEP HD and 1337 kAm^{-1} for the HEP HD. A minor deficiency in magnetic properties in the LEP HD magnet was revealed by statistical analyses, which showed a better texture orientation for the HEP HD magnet. The results indicated a slightly lower remanent magnetization and reduced squareness for the LEP HD magnet.

We have shown that significantly lower energy consumption can produce the hot-deformed magnet if a proper fabrication method is applied. Further studies are under discussion to resolve the mechanism of texture formation during low energy processing and further improve HD magnets' magnetic properties.

6. ACKNOWLEDGEMENTS

This work was supported by projects ID PR-08336, P2 0084, of the Slovenian Research Agency.

7. REFERENCES

[1] M. Sagawa, K. Hiraga, H. Yamamoto, and Y. Matsuura, *Permanent magnet materials based on the rare earth-iron-boron tetragonal compounds (invited)*, IEEE Trans. Magn., Vol. 20–5 (1984) 1584–1589.

[2] J. J. Croat, J. F. Herbst, R. W. Lee, F. E. Pinkerton, *High-energy product Nd-Fe-B permanent magnets*, Appl. Phys. Lett., Vol. 44–1 (1984) 148–149.

[3] Y. Hou, D. J. Sellmyer, *Magnetic nanomaterials: Fundamentals synthesis and applications*, Wiley-VCH Verlag GmbH, 2017.

[4] T. Zhang et al., *Hot-deformed Nd-Fe-B magnets fabricated by dynamic loading with a high maximum energy product*, Intermetallics, Vol. 73 (2016) 67–71.

[5] T. Saito, M. Fujita, T. Kuji, K. Fukuoka, and Y. Syono, *The development of high-performance Nd-Fe-Co-Ga-B die upset magnets*, J. Appl. Phys., Vol. 83–11 (1998) 6390–6392.

[6] K. Hono and H. Sepehri-Amin, *Strategy for high-coercivity Nd-Fe-B magnets*, Scr. Mater., Vol. 67–6 (2012) 530–535.

[7] M. Yue, M. Tian, J. X. Zhang, D. T. Zhang, P. L. Niu, F. Yang, *Microstructure and magnetic properties of anisotropic Nd-Fe-B magnets produced by spark plasma sintering technique*, Mater. Sci. Eng. B Solid-State Mater. Adv. Technol., Vol. 131/1–3 (2006) 18–21.

[8] U. M. R. Seelam et al., *Coercivity of the Nd-Fe-B hot-deformed magnets diffusion-processed with low melting temperature glass-forming alloys*, J. Magn. Magn. Mater., Vol. 412 (2016) 234–242.

[9] M. Soderžnik, M. Korent, K. Žagar Soderžnik, M. Katter, K. Üstüner, S. Kobe, *High-coercivity Nd-Fe-B magnets obtained with the electrophoretic deposition of submicron TbF_3 followed by the grain-boundary diffusion process*, Acta Mater., Vol. 115 (2016) 278–284.

[10] D. Givord, H. S. Li, J. M. Moreau, *Magnetic properties and crystal structure of $Nd_2Fe_{14}B$*, Solid State Commun., Vol. 50–6 (1984) 497–499.

[11] X. Tang, H. Sepehri-Amin, T. Ohkubo, K. Hono, *Suppression of non-oriented grains in Nd-Fe-B hot-deformed magnets by Nb doping*, Scr. Mater., Vol. 147 (2018) 108–113.

[12] Y. H. Hou, Y. L. Huang, Z. W. Liu, D. C. Zeng, S. C. Ma, and Z. C. Zhong, *Hot deformed anisotropic nanocrystalline NdFeB based magnets prepared from spark plasma sintered melt-spun powders*, Mater. Sci. Eng. B Solid-State Mater. Adv. Technol., Vol. 178–15 (2013) 990–997.

[13] O. Gutfleisch, *Controlling the properties of high energy density permanent magnetic materials by different processing routes*, J. Phys. D. Appl. Phys., Vol. 33–17 (2000) 157–172.

[14] R. K. Mishra, E. G. Brewer, R. W. Lee, *Grain growth and alignment in hot deformed Nd-Fe-B magnets*, J. Appl. Phys., Vol. 63–8 (1988) 3528–3530.

[15] R. W. Lee, *Hot-pressed neodymium-iron-boron magnets*, Appl. Phys. Lett., Vol. 46–8 (1985) 790–791.

[16] R. W. Lee, E. G. Brewer, N. A. Schaffel, M*agnets*, IEEE Trans. Magn., Vol. M–5 (1985) 1958–1963.

[17] X. Tang et al., *Relationship between the thermal stability of coercivity and the aspect ratio of grains in Nd-Fe-B magnets: experimental and numerical approaches*, Acta Mater., Vol. 183 (2020) 408–417.

[18] J. Liu et al., *Grain size dependence of coercivity of hot-deformed Nd-Fe-B anisotropic magnets*, Acta Mater., Vol. 82 (2015) 336–343.

[19] X. D. Xu et al., *Comparison of coercivity and squareness in hot-deformed and sintered magnets produced from a Nd-Fe-B-Cu-Ga alloy*, Scr. Mater., Vol. 160 (2019) 9–14.

[20] H. Sepehri-Amin, Y. Une, T. Ohkubo, K. Hono, M. Sagawa, *Microstructure of fine-grained Nd-Fe-B sintered magnets with high coercivity*, Scr. Mater., Vol. 65–5 (2011) 396–399.

[21] J. Liu et al., *Effect of Nd content on the microstructure and coercivity of hot-deformed Nd-Fe-B permanent magnets*, Acta Mater., Vol. 61–14 (2013) 5387–5399.

[22] M. Soderžnik, B. Ambrožič, K. Žagar Soderžnik, M. Korent, *Limits of grain boundary engineering in nanocrystalline Nd-Fe-B melt-spun ribbons*, Mater. Lett., Vol. 264 (2020) 20–22.

[23] J. Liu, H. Sepehri-Amin, T. Ohkubo, K. Hioki, A. Hattori, K. Hono, *Microstructure evolution of hot-deformed Nd-Fe-B anisotropic magnets*, J. Appl. Phys., Vol. 115–17 (2014) 15–18.

[24] M. Soderžnik et al., *Magnetization reversal process of anisotropic hot-deformed magnets observed by magneto-optical Kerr effect microscopy*, J. Alloys Compd., Vol. 771 (2019) 51–59.

[25] L. H. Lewis, Y. Zhu, D. O. Welch, L. Henderson, *Evidence for reversal by nucleation in REFeB die upset magnets Evidence for reversal by nucleation in RE-Fe-B die-upset*, Vol. 6235–1994 (2012) 9–12.

[26] H. Sepehri-Amin et al., *Microstructure and temperature-dependent of coercivity of hot-deformed Nd-Fe-B magnets diffusion processed with Pr-Cu alloy*, Acta Mater., Vol. 99 (2015) 297–306.

[27] K. Hioki, T. Takano, T. Yamamoto, *Influence of Process Conditions on the Magnetic Properties for Hot Deformed Magnets*, Denki-Seiko[Electric Furn. Steel], Vol. 79–2 (2008) 119–125.

[28] M. Korent et al., *Magnetic properties and microstructure evolution of hot-deformed Nd-Fe-B magnets produced by low-pressure spark-plasma sintering*, J. Magn. Magn. Mater., Vol. 515 (2020) 2–7.

[29] J. Trapp, B. Kieback, *Fundamental principles of spark plasma sintering of metals: part I–Joule heating controlled by the evolution of powder*

resistivity and local current densities, Powder Metall., Vol. 62–5 (2019) 297–306.

[30] J. W. Carson, B. H. Pittenger, *Advanced Aluminum Powder Metallurgy Alloys and Composites*, ASM Handb. Vol. 7 Powder Met. Technol. Appl., Vol. 7 (1998) 287–301.

[31] Z. H. Zhang, Z. F. Liu, J. F. Lu, X. B. Shen, F. C. Wang, Y. D. Wang, *The sintering mechanism in spark plasma sintering - Proof of the occurrence of spark discharge*, Scr. Mater., Vol. 81 (2014) 56–59.

[32] N. Chawake, L. D. Pinto, A. K. Srivastav, K. Akkiraju, B. S. Murty, *On Joule heating during spark plasma sintering of metal powders*, Scr. Mater., Vol. 93 (2014) 52–55.

[33] X. Q. Li, L. Li, K. Hu, Z. C. Chen, S. G. Qu, C. Yang, *Microstructure and magnetic properties of anisotropic Nd-Fe-B magnets prepared by spark plasma sintering and hot deformation*, Trans. Nonferrous Met. Soc. China (English Ed.), Vol. 24–10 (2014) 3142–3151.

[34] T. Tomše et al., *A spark-plasma-sintering approach to the manufacture of anisotropic Nd-Fe-B permanent magnets*, J. Magn. Magn. Mater., Vol. 502 (2020) 166504.

[35] Y. Zhang et al., *Squareness factors of demagnetization curves for multi-main-phase Nd-Ce-Fe-B magnets with different Ce contents*, J. Magn. Magn. Mater., Vol. 487 (2019) 165355.

[36] S. Liu, N. H. Kang, L. Feng, S. H. Lee, J. H. Yu, and J. G. Lee, *Anisotropic Nanocrystalline Nd-Fe-B-Based Magnets Produced by Spark Plasma Sintering Technique*, IEEE Trans. Magn., Vol. 51–11 (2015) 18–21.

[37] Z. H. Hu, J. Li, L. H. Chu, Y. Liu, *Effect of hot deformation temperature on the magnetic and mechanical properties of NdFeB magnets prepared by spark plasma sintering*, J. Magn. Magn. Mater., Vol. 323–1 (2011) 104–107.

[38] X. Tang, H. Sepehri-Amin, T. Ohkubo, K. Hioki, A. Hattori, K. Hono, *Coercivities of hot-deformed magnets processed from amorphous and nanocrystalline precursors*, Acta Mater., Vol. 123 (2017) 1–10.

[39] F. Wang, W. Shen, J. Fan, J. Du, K. Chen, J. P. Liu, *Strong texture in nanograin bulk Nd-Fe-B magnets via slow plastic deformation at low temperatures*, Nanoscale, Vol. 11–13 (2019) 6062–6071.

[40] M. Zhu, W. Li, *Texture formation mechanism and constitutive equation for anisotropic thermorheological rare-earth permanent magnets*, AIP Adv., Vol. 7–5 (2017) 056236-6.

[41] L. Li, C. D. Graham, *The Origin of Crystallographic Texture Produced During Hot Deformation in Rapidly-Quenched NdFeB Permanent Magnets*, IEEE Trans. Magn., Vol. 28–5 (1992) 2130–2132.

[42] M. Leonowicz, H. A. Davies, *Effect of Nd content on induced anisotropy in hot deformed FeNdB magnets*, Mater. Lett., Vol. 19/5–6 (1994) 275–279.

[43] E. Castle, R. Sheridan, W. Zhou, S. Grasso, A. Walton, M. J. Reece, *High coercivity, anisotropic, heavy rare earth-free Nd-Fe-B by Flash Spark Plasma Sintering*, Sci. Rep., Vol. 7–1 (2017) 1–12.

[44] H. R. Cha, K. W. Jeon, J. H. Yu, H. W. Kwon, Y. Do Kim, J. G. Lee, *Coercivity enhancement of hot-deformed Nd-Fe-B magnet by grain boundary diffusion process using the reaction of NdHxand Cu nanopowders*, J. Alloys Compd., Vol. 693 (2017) 744–748.

[45] W. Yin, R. Chen, X. Tang, J. Ju, A. Yan, *Effect of pressless heat treatment on the magnetic performance and microstructure of hot-deformed Nd-Fe-B magnet*, J. Magn. Magn. Mater., Vol. 482 (2019) 9–13.

[46] E. A. Périgo, H. Takiishi, C. C. Motta, R. N. Faria, *Microstructure and squareness factor: A quantitative correlation in (Nd, Pr)FeB sintered magnets*," J. Appl. Phys., Vol. 102–11 (2007).

ꕥ

СИНТЕРОВАЊЕ ТОПЛО ИЗМИЈЕЊЕНИХ Nd-Fe-B МАГНЕТА ПУТЕМ НИСКОЕНЕРГЕТСКЕ ИСКРИЧНЕ ПЛАЗМЕ

Сажетак: У овом раду представљамо новоразвијену, економски ефикасну методу процесирања Nd-Fe-B магнета ријетких земаља, базирану на синтеровању искричне плазме. То нам омогућава да сачувамо технолошки битне карактеристике произведених магнета искористивости око 30% енергије у поређењу са конвенционалним SPS процесом. Магнет анизотропичне структуре сачињен је од MQU F комерцијалне траке уз потрошњу ниске енергије (0,37 MJ) током процеса деформације и у поређењу са конвенционалном припремљеним топло деформисаним магнетом, који користи три пута више енергије (1,2 MJ). Оба магнета накнадно су каљена на температури од 650 °C, 120 минута у вакууму. Након процеса каљења, топло

измијењени магнет процесиран нискоенергетски (LEP), показао је магнетну коерцитивност од 1.327 kAm^{-1} и реманентни магнетизацију од 1.27 T. У поређењу, високоенергетски процес топло измијењених магнета (HEP) имао је коерцитивност 1.337 kAm^{-1} и реманентну магнетизацију од 1.31 T. Завршена микроструктурална карактеризација и детаљна статистичка анализа показују бољу текстуалну оријентацију за HEP топло измијењене магнете процесиране употребом високе енергије, што је и основни разлог за разлику у реманентној магнетизацији између два топло измијењена магнета. Резултат показује да, поред тога што је LEP топло измијењени магнет био процесиран три пута нижом употребом енергије него у типичним процесима топлих измјена, максималан енергетски производ је само 8% нижи од максималног енергетског производа HEP топло измијењеног магнета.

Кључне ријечи: топло измијењени Nd-Fe-B магнети, нискоенергетски процеси топлих измјена, синтеровање искричне плазме, статистичке анализе, електронска микроскопија.

Paper received: 20 September 2021
Paper accepted: 31 October 2021